LANGMUIR
Cite This: *Langmuir* 2018, 34, 1601−1612
Article
pubs.acs.org/Langmuir

Dynamically Cross-Linked Self-Assembled Thermoresponsive Microgels with Homogeneous Internal Structures

Eva Mueller,[†] Richard J. Alsop,[‡] Andrea Scotti,[§] Markus Bleuel,[∥,⊥] Maikel C. Rheinstädter,[‡] Walter Richtering,[§] and Todd Hoare*[,†]

[†]Department of Chemical Engineering, McMaster University, 1280 Main Street W, Hamilton, Ontario L8S 4L7, Canada
[‡]Department of Physics and Astronomy, McMaster University, 1280 Main Street W, Hamilton, Ontario L8S 4M1, Canada
[§]Department of Physical Chemistry (IPC), RWTH Aachen, Landoltweg 2, 52074 Aachen, Germany
[∥]Neutron-Condensed Matter Science Group, National Institute of Standards and Technology (NIST), 100 Bureau Drive, Gaithersburg, Maryland 20899, United States
[⊥]Department of Materials Science and Engineering, University of Maryland, College Park, Maryland 20742-2115, United States

Supporting Information

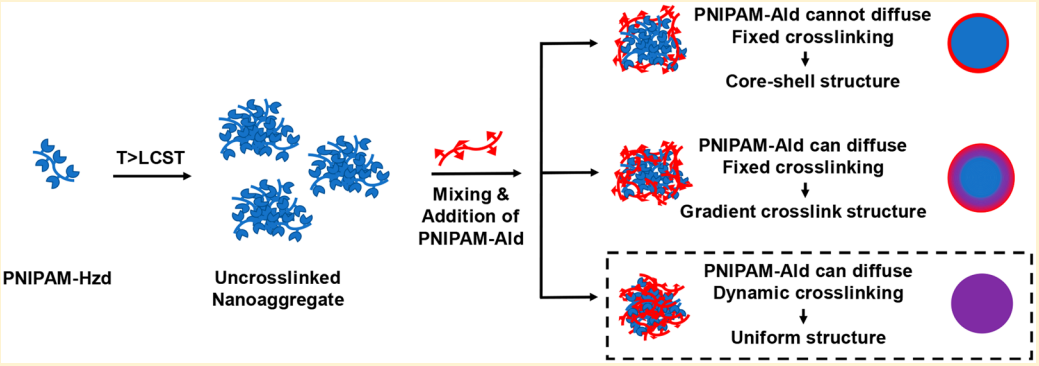

ABSTRACT: The internal morphology of temperature-responsive degradable poly(*N*-isopropylacrylamide) (PNIPAM) microgels formed via an aqueous self-assembly process based on hydrazide and aldehyde-functionalized PNIPAM oligomers is investigated. A combination of surface force measurements, small angle neutron scattering (SANS), and ultrasmall angle neutron scattering (USANS) was used to demonstrate that the self-assembled microgels have a homogeneously cross-linked internal structure. This result is surprising given the sequential addition process used to fabricate the microgels, which was expected to result in a densely cross-linked shell−diffuse core structure. The homogeneous internal structure identified is also significantly different than conventional microgels prepared via precipitation polymerization, which typically exhibit a diffuse shell−dense core structure. The homogeneous structure is hypothesized to result from the dynamic nature of the hydrazone cross-linking chemistry used to couple with the assembly conditions chosen that promote polymer interdiffusion. The lack of an internal cross-linking gradient within these degradable and monodisperse microgels is expected to facilitate more consistent drug release over time, improved optical properties, and other potential application benefits.

INTRODUCTION

Microgels, colloidal networks of cross-linked water-soluble polymers with dimensions <1 μm, have been demonstrated to be useful materials in a wide range of biomedical and environmental applications. In particular, temperature-responsive microgels and nanogels based on poly(*N*-isopropylacrylamide) (PNIPAM) have attracted significant research interest due to their ability to change their diameter,[1−4] hydrophobicity,[5] pore size,[6] and surface charge[7,8] as a function of temperature, the so-called volume phase transition temperature (VPTT) behavior. These thermally switchable properties have been applied in drug delivery[9] (to target locally hotter areas in the body, such as poorly vascularized but quickly metabolizing cancerous sites[10,11]), bioseparations[12,13] (to reversibly adsorb/desorb a target molecule), membranes[14,15] (to open or close pores), nanoswitches[16] (to oscillate on/off responses in microfluidic channels), and other applications.[4,17] Each of these applications works due to some combination of the reduced hydrophilicity and/or the reduced pore size observed upon heating with the former governing the strength of interactions between the microgel and more hydrophobic molecules[18,19] and the latter governing the diffusivity of molecules through the gel network.[20]

The swelling properties and the transition temperature responses of microgels are governed by not only the chemistry

Received: October 20, 2017
Revised: December 20, 2017
Published: December 20, 2017

DOI: 10.1021/acs.langmuir.7b03664
Langmuir 2018, 34, 1601−1612

but also the internal microgel structure. The internal structure regulates the speed/degree of swelling,[21−23] the breadth of the volume phase transition (less internally heterogeneous particles have narrower transitions),[24,25] the rate of intraparticle diffusion,[26] the ease of microgel functionalization,[27] and the capacity of the microgels for the uptake/release of small molecules.[6,28] The internal structure of microgels is most commonly studied using small-angle neutron scattering (SANS) in dilute suspensions, although static light scattering can also give some insight.[29] Direct modeling expressions for the scattering intensity distribution have been developed to describe structural changes induced by changes in temperature,[30−32] cross-linking density,[33] or particle size[29,30] as well as inherent compositional gradients resulting from the synthetic conditions used (e.g., batch, semi batch or controlled monomer feed).[34]

The internal structure of microgels is directly related to the method by which the microgels are synthesized. Conventional PNIPAM microgels are made by a precipitation polymerization process[35] in which NIPAM monomers are polymerized with *N*,*N*′-methylenebis(acrylamide) (MBA) cross-linker using a water-soluble free radical initiator (i.e., potassium sulfate) at a temperature above the lower critical solution temperature (LCST) of PNIPAM to drive particle formation.[24,36] Other monomers may be copolymerized to obtain microgels with desired properties and the process may be carried out in batch, semibatch, or continuous modes.[24] The resulting microstructure of the microgels produced using this conventional technique has been shown to relate directly to the copolymerization ratios between the constituent monomers and cross-linkers used to prepare the microgel.[37] For example, because the MBA cross-linker typically used to prepare microgels reacts faster than NIPAM, the core of the resulting microgel is more densely cross-linked than the shell, resulting in a "fuzzy sphere" nanostructure.[1] The fuzzy sphere internal structure of conventional PNIPAM microgels was further studied and formally quantified with a small angle neutron scattering (SANS) model by Stieger et al.[30] Additionally, Geisel et al. investigated and indirectly confirmed the core−corona structure of PNIPAM-copolymerized with methacrylic acid (MAA) microgels using interface/surface force measurements.[38] This inhomogeneous structure makes the prediction of drug binding,[18] swelling responses,[39] and other key microgel properties challenging, although also offering opportunities to leverage these structures in specific applications (e.g., bioconjugation[3]).

Given that copolymerization kinetics govern the microgel morphology via precipitation polymerization, it is possible to manipulate the feed rate of the monomers/cross-linkers within the scope of the conventional precipitation process to create uniformly cross-linked particles. For example, Acciaro et al. have prepared homogeneous PNIPAM microgels by using a continuous reactor to maintain the concentrations of monomer and cross-linker constant,[21] Du's group copolymerized an unprotected catechol monomer that could self-cross-link to create a more homogeneous internal structure,[40] and we have demonstrated the capacity to create uniform functional group distributions in microgels using semibatch delivery of the functional monomer.[41] In all cases, the homogeneously cross-linked or functionalized microgels showed significantly different optical and swelling properties relative to conventional batch polymerized microgels, showing the importance of controlling and understanding the internal morphology of microgels in designing particles for applications.

Alternately, to avoid the dominance of free radical copolymerization kinetics on the morphology of the resulting microgels, two-step microgel fabrication techniques have been reported in which a preformed PNIPAM polymer or oligomer is heated above its LCST to form a nanoaggregate followed by cross-linking to stabilize that aggregate into a microgel. Multiple post-cross-linking strategies including UV irradiation[42,43] and self-condensation of pendant methoxysilyl groups[44] have been reported to create microgels from the nanoaggregates with the distribution of cross-linking sites governed by UV light penetration and/or the surface activity of the precursor polymer(s) in the former case and the self-association of the hydrophobic methoxysilyl groups in the latter case.

However, particularly in the context of biological applications, controlling degradability remains a challenge with both the conventional synthesis approach as well as these nanoaggregation stabilization strategies. In the former case, there is no direct way to control the molecular weight of degradation products (even if degradable cross-linkers are used) to ensure the ultimate clearance of the materials; in the latter case, the bonds formed are nondegradable. Alternate methods such as prepolymer cross-linking inside inverse emulsions allows for both homogeneous internal morphologies as well as degradation into well-defined products;[45] however, this approach typically results in nonuniform particle size distributions.[46] Microfluidics can be utilized to produce more uniform microgels with specific flow-focusing techniques[47] but typically results in larger particle sizes in the micron size range instead of the nanoscale.

Recently, we have developed a novel method to create degradable and monodisperse microgels using a thermally driven self-assembly approach mimicking the conventional microgel fabrication process but using well-defined hydrazide and aldehyde-functionalized PNIPAM oligomers instead of the monomers as the building blocks. Mixing the hydrazide (PNIPAM-Hzd) and aldehyde (PNIPAM-Ald)-functionalized oligomers results in the formation of degradable hydrazone cross-links;[2] by maintaining the molecular weight of those oligomers below the kidney clearance limit, we can facilitate renal clearance of the synthetic polymer-based microgel network following degradation of the hydrazone cross-links. These degradable analogues of conventional thermoresponsive microgels can be fabricated rapidly (<10 min) using a highly scalable method to generate colloidally stable, noncytotoxic microgels with sizes in the 200−300 nm range, high monodispersity, and controllable swelling responses.[2] Furthermore, given that the stoichiometry and sequence of addition of PNIPAM-Hzd and PNIPAM-Ald are asymmetric during the assembly process, residual functional groups are available in the microgel to enable covalent "layer-by-layer" (LbL) assembly of the reactive prepolymers templated from the initially fabricated microgel, previously only demonstrated on microgels via polyelectrolyte interactions.[48] Interestingly, in such previous microgel studies, the soft and porous nature of microgels enabled significant interpenetration of lower molecular weight polyelectrolyte into the microgels[49] with the reversible ionic interactions between the charged additive polymer and the oppositely charged microgel enabling the transport of the polymer into the microgel core.[50] We have previously demonstrated the efficacy of the proposed covalent LbL approach for fabricating thin film hydrogels with tunable thicknesses[51] but have not yet demonstrated a similar effect on the nanoscale.

Given that our new microgel fabrication method involves controlled thermoaggregation of the hydrazide-functionalized

DOI: 10.1021/acs.langmuir.7b03664
Langmuir 2018, 34, 1601−1612

prepolymer at a temperature above its LCST followed by the addition of the aldehyde-functionalized prepolymer, we hypothesized that mass transfer considerations would limit the diffusion of PNIPAM-Ald into the collapsed PNIPAM-Hzd aggregate prior to hydrazone bond formation (which is rapid in aqueous conditions[52]) to result in a dense shell/disperse core structure, the inverse of the conventional microgel morphology. However, to-date we do not have evidence supporting this hypothesized microstructure. In addition, the dynamic nature of the hydrazone bond means that initial cross-links formed during synthesis may be broken and reformed over time, such that a homogenization of the cross-link distribution at room temperature at T < VPTT is theoretically possible even if the interdiffusion of the two polymers during the T > VPTT fabrication step is indeed rate-limited. Similarly, for the covalent LbL surface modification steps performed on prefabricated microgels at T > VPTT, the dynamic cross-linking chemistry may permit interdiffusion of the added polymer into the gel structure over time (as observed with the polyelectrolyte LbL assemblies[49]) despite the fast and multidentate covalent cross-linking anticipated between the added functional polymer and residual surface or near-surface complementary functional groups.

Herein, we investigate the internal morphology of these self-assembled PNIPAM microgels with or without subsequent LbL modification using a combination of surface force measurements, small-angle neutron scattering (SANS), and ultrasmall-angle neutron scattering (USANS). In contrast to our initial hypothesis about the structure of these oligomeric self-assembled microgels, both Langmuir trough experiments and SANS/USANS (both on the microgels as a whole as well as contrast-matched SANS highlighting the individual distributions of PNIPAM-Hzd and PNIPAM-Ald) indicate that the self-assembled microgels feature highly uniform internal morphologies, a result we attribute to the dynamic instead of static nature of the hydrazone cross-links formed. As such, the oligomeric self-assembly approach not only leads to degradable microgels but also highly homogeneous microgel structures which may be of significant benefit in optical, drug delivery, and other applications in which uniform cross-link densities should yield more uniform properties.

EXPERIMENTAL SECTION

Materials. *N*-isopropylacrylamide (NIPAM, 99%), acrylic acid (AA, 99%), thioglycolic acid (98%), aminoacetaldehyde dimethyl acetal (99%), sodium cyanoborohyride (95%), 2,2,6,6-tetramethyl-1-piperidinyloxy (TEMPO, 98%), and methacryloyl chloride (purum) were purchased from Sigma-Aldrich (Oakville, Canada). NIPAM was purified by dissolving 1 g/mL in toluene at 60 °C, adding a 2:3 ratio of hexane/toluene, placing the solution in an ice bath for 1−2 h, filtering/rinsing with hexanes, and drying the recrystallized NIPAM monomer under N_2 overnight. Adipic acid dihydrazide (ADH, Alfa Aesar, 98%), *N*′-ethyl-*N*-(3-(dimethylamino)propyl)-carbodiimide (EDC, Carbosynth, Compton CA, commercial grade), 2,2-azobisisobutryic acid dimethyl ester (AIBMe, Wako Chemicals, 98.5%), and ethanol (Commercial Alcohols, Brampton, Ontario) were purchased and used without further purification. Milli-Q grade distilled deionized water (DIW) was used for all experiments. Deuterium oxide (99.9 atom % D) was purchased from Sigma-Aldrich (Oakville, Canada) for use in neutron scattering experiments. *N*-decane (Sigma-Aldrich, 99%) was purchased and triple-columned with aluminum oxide prior to use.

Prepolymer Synthesis. Hydrazide-functionalized (PNIPAM-Hzd) and aldehyde-functionalized (PNIPAM-Ald) prepolymers were synthesized using the previously reported protocols.[2] Briefly, PNIPAM-Hzd was prepared via free radical copolymerization of NIPAM (4.5 g) and acrylic acid (0.5 g) in 20 mL of ethanol using thioglycolic acid (TGA, 80 μL) as the chain transfer agent and 2,2-azobisisobutyric acid dimethyl ester (AIBME, 0.056 g) as the initiator (reaction temperature = 60 °C). Gel permeation chromatography (GPC) using a Waters 590 HPLC pump, three Waters Styragel columns (HR2, HR3, HR4; 30 cm × 7.8 mm (i.d); 5 μm particles) at 40 °C, a Waters 410 refractive index detector operating at 35 °C, and DMF as the solvent indicated that the resulting polymer had a molecular weight of 21.6 kDa, while base-into-acid conductometric titration indicated a stoichiometric incorporation of acrylic acid (∼15 mol %) into the polymer. Subsequently, the acrylic acid residues were conjugated using carbodiimide chemistry with a 5-fold excess of adipic acid dihydrazide, resulting in an overall conversion of 95% of acrylic acid residues to hydrazide functionalities (i.e., ∼ 14 mol % of the total monomer residues were functionalized with a hydrazide group). Deuterated PNIPAM-Hzd (d-PNIPAM-Hzd) was similarly prepared by substituting NIPAM with d7-PNIPAM (Polymer Source, Montreal, PQ) in the recipe with base-into-acid conductometric titration indicating the same stoichiometric (∼15 mol % total monomer) incorporation of acrylic acid into the polymer and ∼95% conversion of those acrylic acid residues into hydrazide groups following carbodiimide coupling.

PNIPAM-Ald was prepared by copolymerizing NIPAM (4.5 g) with *N*-(2,2-dimethoxyethyl)methacrylamide[53] (DMEMAm, 0.95 g) using the same polymerization conditions used for the hydrazide polymer, resulting in a polymer with a molecular weight of ∼15.1 kDa via GPC. Subsequently, acid hydrolysis of the pendant acetal groups in DMEMAm into aldehyde groups was performed by dissolving the initial polymer in 1 M HCl and hydrolyzing over 24 h, resulting in 12 mol % of total monomer residues in the polymer bearing aldehyde groups. All polymers were dialyzed against Milli-Q water for six cycles of at least 6 h and lyophilized for storage.

Microgel Particle Size Measurements. Dynamic light scattering measurements were performed using a Brookhaven 90Plus particle analyzer running Particle Solutions Software (Version 2.6, Brookhaven Instruments Corporation), using a 659 nm laser and a 90° detection angle. Each measurement was performed at a count rate between 200 and 500 kilocounts/s for 2 min and repeated at least six times. The intensity-weighted particle sizes and polydispersities were reported as averages of these six replicate measurements with the reported error representing the standard deviation of these replicates.

Microgel Fabrication. Oligomer self-assembled microgels were prepared following our previously reported self-assembly/precipitation protocol (Figure 1).[2] Both PNIPAM-Hzd and PNIPAM-Ald were dissolved at 1 wt % in D_2O or a mixture of D_2O/H_2O appropriate for index matching (see the SANS section for details on how this ratio was chosen). The PNIPAM-Hzd solution (5 mL) was then heated to a temperature above its lower critical solution temperature (LCST) to create stable nanoaggregates, after which the PNIPAM-Ald solution was added dropwise (∼1−2 drops per second) at either 5 or 20% mass PNIPAM-Ald/mass of PNIPAM-Hzd to stabilize the nanoaggregate via a hydrolytically labile hydrazone bond. All self-assemblies were performed at a reaction temperature of 70 °C, well above the LCST of PNIPAM-Hzd (∼56 °C) to ensure efficient nanoaggregate formation. The mixture was magnetically stirred (350 rpm) at 70 °C for 15 min following PNIPAM-Ald addition to ensure cross-linking prior to cooling.

To assess the impact of adding additional functional polymer following the initial assembly process (i.e., "layer-by-layer" self-assembly), the preformed microgel suspensions were cooled overnight and then reheated to 70 °C. Either PNIPAM-Hzd or PNIPAM-Ald at a concentration of 5 or 20% mass/mass of initial PNIPAM-Hzd was then added as described above for the initial PNIPAM-Ald cross-linking step, with the process repeated as desired to add additional "layers" to the assembly.

Small-Angle Neutron Scattering (SANS). SANS experiments were conducted using the 30 m SANS NGB30 at the NIST Center for Neutron Research (NCNR, Gaithersburg, MD). Sample-to-detector distances of 1, 4, and 13 m were used in conjunction with neutrons of wavelength 6 Å, while the lens geometry was also used at the 13 m detector distance with 8.4 Å wavelength neutrons to expand the accessible q range. The microgels were self-assembled in D_2O as described in the previous section and loaded into NCNR's custom titanium/quartz

DOI: 10.1021/acs.langmuir.7b03664
Langmuir 2018, 34, 1601−1612

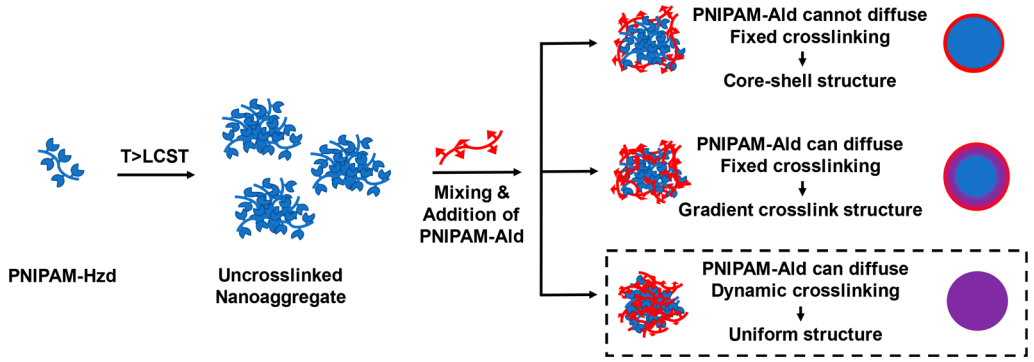

Figure 1. Schematic of precipitation/self-assembly process used to fabricate degradable microgels from functional PNIPAM oligomers and anticipated structures of resulting microgels depending on the diffusibility of the PNIPAM-Ald cross-linker and the permanence of the cross-links formed. The homogeneous morphology is consistent with the structural characterization results.

sample holders (diameter 19 mm and path length 2 mm) without further dilution. The internal gap thickness of the sample cell was 2 mm, which corresponds to ~800 μL of test solution. Three microgels were assessed at four temperatures (25, 32, 37, and 45 °C) spanning the volume phase transition temperature (VPTT) of PNIPAM-based microgels: (1) 0.05 Ald/Hzd microgels (prepared with a 1 wt % PNIPAM-Hzd starting solution), (2) 0.20 Ald/Hzd microgels (1 wt % PNIPAM-Hzd starting solution), and (3) 0.05 Ald/Hzd microgels (2 wt % PNIPAM-Hzd starting solution). In addition, four layer-by-layer microgels were assembled in the sequences listed below and measured at 25 °C only to assess the mass distribution in each microgel as a result of the layer-by-layer assembly process: (1) 0.05 Ald/Hzd microgel + PNIPAM-Hzd, (2) 0.05 Ald/Hzd microgel + PNIPAM-Ald, (3) 0.05 Ald/Hzd microgel + PNIPAM-Hzd + PNIPAM-Hzd, and (4) 0.05 Ald/Hzd microgel + PNIPAM-Hzd + PNIPAM-Ald. Note that each "+ Polymer" addition step listed above involves cooling the sample overnight, reheating to the assembly temperature of 70 °C, and adding the next polymer in sequence at the concentrations listed above. Additional measurements were also performed on PNIPAM-Hzd precursor polymer solutions at the same concentration and temperature used for microgel self-assembly, allowing for direct correlation between the structure of the nanoaggregate before and after cross-linking. The low q range data were acquired by counting for ~20 min using the 13 m distance, the medium q range data were acquired by counting for ~15 min using the 4 m distance, and the high q range data were acquired for ~5 min using the 1 m detection distance. The three ranges were merged using the DAVE on-site data reduction tool and standard Igor Pro macros.[54,55]

The contrast matching experiment on the self-assembled PNIPAM microgels was performed by fabricating microgels using d7-PNIPAM-Hzd as the seed polymer and (hydrogenated) PNIPAM-Ald as the cross-linking polymer (0.2 Hzd/Ald polymer mass ratio) with the ratio of D_2O/H_2O in the suspending solvent changed in order to match one of the two constituent polymers. The match points were first calculated based on the atomic composition to predict the theoretical scattering length density for each of the polymers, corresponding to theoretical match points 67:33 (v/v) D_2O/H_2O for d7-PNIPAM-Hzd and 21:79 (v/v) D_2O/H_2O for hydrogenated PNIPAM-Ald. These values were refined by conducting scattering experiments both at the calculated match point as well as ±10% solvent mixtures from this calculated match point with the experimental D_2O/H_2O ratio producing zero scattering determined by regression to be 63:37 D_2O/H_2O for d7-PNIPAM-Hzd and 22:78 D_2O/H_2O for PNIPAM-Ald. Microgels were then self-assembled as described in the previous section in the matched solvents to ensure the total microgel concentration was constant for each experiment. SANS experiments were conducted as previously described for the noncontrast matched samples.

Ultrasmall Angle Neutron Scattering (USANS). USANS experiments were conducted on the contrast-matched microgels using the BT5 USANS at the NIST Center for Neutron Research (NCNR, Gaithersburg, MD).[56] The neutron wavelength used was 2.4 Å ± 6%, with the q range spanning between ~0.00003 to 0.002 Å^{-1} to slightly overlap the lower end of the accessible q range from SANS (0.001 Å^{-1}) and allow for efficient stitching/scaling of the data using the DAVE on-site data reduction tool. Samples were loaded into the same sample holder used for SANS analysis.

Neutron Scattering Data Analyses. The SANS analysis on the bulk microgels and the contrast-matched microgels was done using Interactive Data Language (IDL) and Igor Pro, using the fuzzy sphere model shown in eq 1

$$I(q) = \frac{\text{scale}}{V}(\Delta\rho)^2\langle A^2(q)\rangle S(q) + \frac{I_{lor}(O)}{1 + (\xi^* q)^m} + bkg \quad (1)$$

where

$$A(q) = \frac{3[\sin(qR) - qR\cos(qr)]}{(qR)^3}\exp\left(\frac{-(\sigma_{fuzzy}q)^2}{2}\right) \text{ and}$$

$$q = \frac{4^*\pi}{\lambda}\sin\left(\frac{\theta}{2}\right)$$

Note that the $\langle\ \rangle$ brackets denote an average over the size distribution, where $\langle A^2(q)\rangle$ represents the form factor $P(q)$, $S(q)$ is the structure factor (for dilute solutions, $S(q) = 1$ for all q), ξ is the correlation length (roughly representing the mesh size of the gel network), σ_{fuzzy} denotes the width of the smeared or "fuzzy" particle surface (which, when set to 0, reduces the expression to that of a homogeneous sphere), m is the Lorentzian exponent, and q is the scattering vector, related to the neutron wavelength (λ) and the scattering angle (θ). Since the instrument resolution causes a smearing of the data, the intrinsic desmearing function in IgorPro (the convolution of $P(q)$ with a Gaussian function) was used to account for smearing effects.[57]

Langmuir Trough. Compression isotherms were recorded and analyzed on the oil–water interface using a KSV-NIMA Langmuir trough with two barriers operating at a speed of 108 mm/min and a platinum Wilhelmy plate to measure the change in interfacial tension from the clean interface to the interface covered with microgel particles. Distilled water (200 mL) was used as the aqueous phase and triple-columned n-decane (200 mL) was used as the oil phase. Low cross-link ratio (0.05 Ald/Hzd polymer mass ratio) or high cross-link ratio (0.20 Ald/Hzd polymer mass ratio) self-assembled microgels were dispersed in the aqueous phase. As the particles were compressed, the change in interfacial tension was measured with the platinum Wilhelmy plate with the measurement converted to a surface pressure using the KSV-NIMA software.

RESULTS

Microgel Particle Size. The hydrodynamic radius and polydispersity of the microgels in a dilute suspension of D_2O, the layer-by-layer assembled microgels in D_2O, and the contrast-matched microgels at the relevant D_2O/H_2O ratios used for the contrast matching experiments at 25 °C (T < VPTT) are listed

DOI: 10.1021/acs.langmuir.7b03664
Langmuir 2018, 34, 1601−1612

Table 1. Dynamic Light Scattering Size and Polydispersity Measurements on Microgels in Solvents Used for SANS/USANS Analysis

microgel description	solvent	radius (nm)	polydispersity
0.05 Ald/Hzd (1 wt %)	D_2O	162 ± 3	0.08 ± 0.01
0.20 Ald/Hzd (1 wt %)	D_2O	145 ± 3	0.11 ± 0.02
0.05 Ald/Hzd (2 wt %)	D_2O	203 ± 9	0.16 ± 0.02
0.05 Ald/Hzd (1 wt %) + PNIPAM-Hzd	D_2O	176 ± 8	0.10 ± 0.01
0.05 Ald/Hzd (1 wt %) + PNIPAM-Hzd + PNIPAM-Hzd	D_2O	166 ± 7	0.15 ± 0.03
0.05 Ald/Hzd (1 wt %) + PNIPAM-Ald	D_2O	166 ± 4	0.13 ± 0.02
0.05 Ald/Hzd (1 wt %) + PNIPAM-Hzd + PNIPAM-Ald	D_2O	268 ± 12	0.21 ± 0.4
d-PNIPAM-Hzd 0.20 Ald/Hzd (1 wt %) (d-PNIPAM-Hzd match)	63 D_2O/37 H_2O	183 ± 16	0.17 ± 0.03
d-PNIPAM-Hzd 0.20 Ald/Hzd (1 wt %) (PNIPAM-Ald match)	22 D_2O/78 H_2O	176 ± 8	0.15 ± 0.04

in Table 1. Note that the solvents chosen for each listed measurement relate directly to those used in the SANS and USANS experiments, such that the sizes measured are directly comparable between the experiments. Relative to the same microgels fabricated in H_2O, the particle sizes measured in D_2O are consistently larger; this is reflective of the higher propensity of D_2O to form hydrogen bonds,[58] which is the driving force for microgel hydration at T < VPTT. However, the trends in size are identical to those observed in H_2O with lower radii observed as the relative amount of PNIPAM-Ald (cross-linker) was increased and higher radii observed when higher concentrations of the PNIPAM-Hzd polymer were used to form the initial nanoaggregate. For the covalent LbL-assembled microgels, adding one additional treatment of PNIPAM-Hzd resulted in a small but significant increase in particle size; however, adding an additional treatment of PNIPAM-Ald or adding sequential additional treatments of PNIPAM-Hzd resulted in no significant change in the particle size (p < 0.05 in either pairwise comparison). This lack of an observed size change would not be anticipated if a true LbL surface assembly (akin to conventional polyelectrolyte LbL assembly) was happening. Instead, we hypothesize that the size results are indicative of a balance between additional cross-linking (restricting swelling) and the introduction of more hydrophilic hydrazide/aldehyde groups (driving swelling) upon the addition of each subsequent functional polymer. Of note, sequential additions of PNIPAM-Hzd followed by PNIPAM-Ald resulted in a much higher particle size of 268 ± 12 and substantially higher polydispersity compared to the other samples tested, suggesting significant interparticle aggregation in this case that was not observed with other samples. In the contrast-matched samples, the microgel size did not significantly change when deuterated d7-PNIPAM-Hzd was used as the building block of the microgel as opposed to protonated PNIPAM-Hzd (p < 0.05).

SANS of PNIPAM-Hzd Nanoaggregates. To gain insight into the mechanism by which the sequential addition process creates self-assembled microgel particles and the structure of the thermally collapsed nanoaggregates that seed the self-assembled microgels, PNIPAM-Hzd precursor polymer solutions (prior to PNIPAM-Ald addition) were tested in D_2O using SANS at 70 °C and 1 or 2 wt %, the temperature and concentrations used in the self-assembly process. The majority of resulting profiles aside from the low q regime could both be fit to the homogeneously cross-linked sphere model (i.e., σ_{fuzzy} = 0 in eq 1) using characteristic radii of 66 nm for 1 wt % PNIPAM-Hzd and 73 nm for 2 wt % PNIPAM-Hzd (Table 2; see raw data and best fit functions in Supporting Information, Figure S1). The higher size of the 2 wt % nanoaggregate is consistent with the larger size of the resulting microgels produced (Table 1), indicating some correlation between the nanoaggregate size and the resulting microgel. These sizes are however substantially smaller than those measured on the same samples via DLS (166 ± 1 and 176 ± 1 nm, respectively), although the high measured polydispersities (~0.3) indicate substantial aggregation in the samples and the intensity weighting of the DLS results consistently overweights the effect of larger particles on the average particle size reported. SANS analysis similarly indicates that both precursor solutions exhibited broad polydispersities of ~31%, with the low q region for both concentration samples showing a constant slope (the green solid lines in Figure S1) indicative of large-scale aggregation.[59] Interestingly, these poorly defined preaggregates can successfully be utilized to create relatively monodisperse microgel particles.

SANS of Self-Assembled PNIPAM Microgels. SANS experiments as a function of temperature were subsequently performed to assess the impact of the PNIPAM-Hzd starting concentration and the ratio between PNIPAM-Ald: PNIPAM-Hzd on the microgel morphology with the results shown in Figure 2. The best fits accomplished with the fuzzy sphere model returned a finite shell thickness of between 2 and 4 nm, a shell thickness at the extreme lower boundary of relevance for the core−shell model (Supporting Information, Figure S2). χ^2values, corresponding to the goodness of fit of the model functions to the experimental data, were similar for both the homogeneously cross-linked model (σ_{fuzzy} = 0) and the core−shell Stieger model at all temperatures evaluated (Table S1); furthermore, the mid-q oscillations that are captured by the fuzzy sphere model[30] are not visible on the SANS profiles of the self-assembled microgels. Together these observations suggest that the additional core−shell terms in the Stieger model are unnecessary for fitting the experimental data, leading us to use the homogeneous model to fit all SANS microgel profiles pre sented in Figure 2. Note that this result lies in sharp contrast to conventionally prepared PNIPAM microgels in which a core−shell model with a significant shell thickness on

Table 2. Best Fit Parameters for Fuzzy Sphere Model Fit of PNIPAM-Hzd Nanoaggregates at 70°C[a]

PNIPAM-Hzd concentration (mg/mL)	σ_{fuzzy}	radius (nm)	polydispersity	ε (nm)	M
1	0	66	0.30	3.0	3.5×10^{-5}
2	0	73	0.31	3.2	6.5×10^{-5}

[a]See Supporting Information Figure S1 for raw data and fit curves.

DOI: 10.1021/acs.langmuir.7b03664
Langmuir 2018, 34, 1601−1612

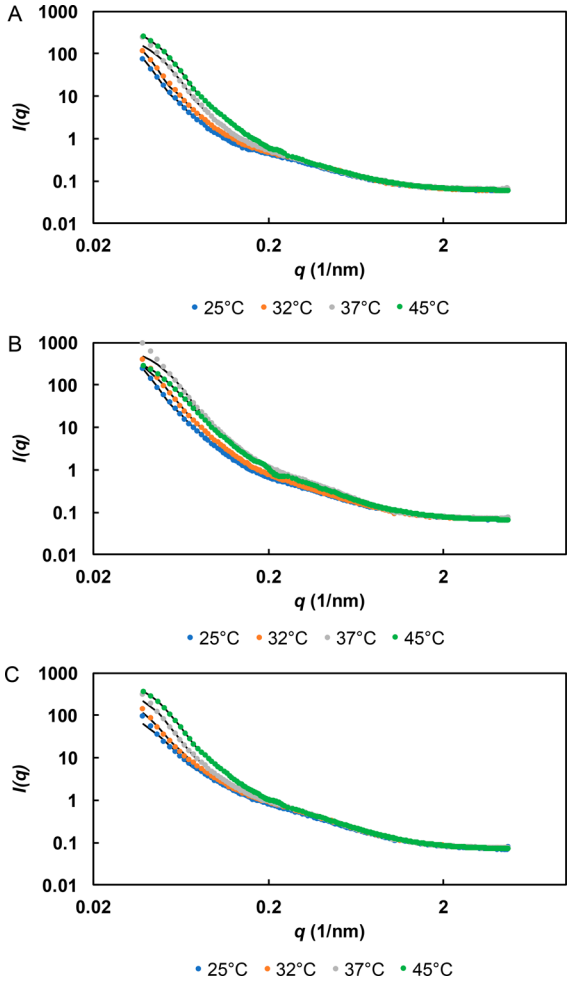

Figure 2. Neutron scattering intensity $I(q)$ as a function of the scattering vector (q) as a function of temperature for (A) 0.05 Ald/Hzd microgel (1 wt % PNIPAM-Hzd); (B) 0.20 Ald/Hzd microgel (1 wt % PNIPAM-Hzd); (C) 0.05 Ald/Hzd microgel (2 wt % PNIPAM-Hzd). Solid black lines represent the fits, and standard deviations of the fits are plotted as error bars.

the order of 14−30 nm (below VPTT) is required to accurately fit the SANS profiles.[30] Figure 3 shows the corresponding key fitting parameters of microgel radius and mesh size as a function of temperature extracted from the homogeneous sphere fits. All fitting parameters (including a summary) for the bulk self-assembled PNIPAM microgels are included in Supporting Information Tables S3 and S4.

In general, the scattering intensity observed increases systematically with temperature as the microgels are heated from below (25 °C) to above (45 °C) their VPTT, consistent with previous studies on thermoresponsive hydrogels[60] and microgels.[30,32,61] Note that slight aggregation above the VPTT occurred particularly in the 0.20 Ald/Hzd (1 wt %) sample (Figure 2B), which is reflected in the somewhat poorer fit achieved at 37 °C and the lower intensity profile observed at 45 °C. This increased intensity as a function of temperature correlates to a discontinuous transition in the best fit microgel radius as a function of temperature (Figure 3A), consistent with (albeit slightly larger in overall magnitude compared to) the dynamic light scattering measurement of the phase transition (Supporting Information, Figure S3). The higher radius in the collapsed state as well as the higher temperature transition measured via DLS relative to SANS can again be attributed to the intensity weighting of the size distribution in DLS; however, the general trends measured via both techniques are highly comparable. The best fit radius of 0.05 Ald/Hzd prepared with 2 wt % PNIPAM-Hzd seed polymer also was significantly higher at lower temperatures compared to microgels prepared with a 1 wt % PNIPAM-Hzd seed polymer (Figure 3A), again consistent with DLS results (Table 1).

Typically, decreases in microgel radius are accompanied by decreases in the correlation length (ε), which is conventionally attributed to represent the mesh size of the network. However, only minimal changes in the correlation length were observed as a function of temperature for the self-assembled microgels with very slight (~0.5 nm) decreases observed between 32 and 37 °C for the two lower cross-link density microgels prepared with a 0.05 Ald/Hzd ratio and no significant change in correlation length observed for the more cross-linked microgel (0.20 Ald/Hzd ratio). The comparative differences between different cross-link density microgels are consistent with the DLS results and the best-fit SANS radius results in which more cross-linked microgels exhibit broader and lower magnitude phase transitions that would result in lower changes in network mesh size as a function of temperature; this is also consistent with observations on conventional (nonhomogenous) microgel particles.[62] However, at least some change in correlation length versus temperature was anticipated for all microgels. We hypothesize this is a result of a change in the network from being more homogeneous to featuring nanophase separated domains upon heating, the size/spacing of which may also be captured in the correlation length parameter. Given the relatively high number of polar hydrazide, aldehyde, or hydrazone functional groups present in the network, the potential for such nanoscale phase

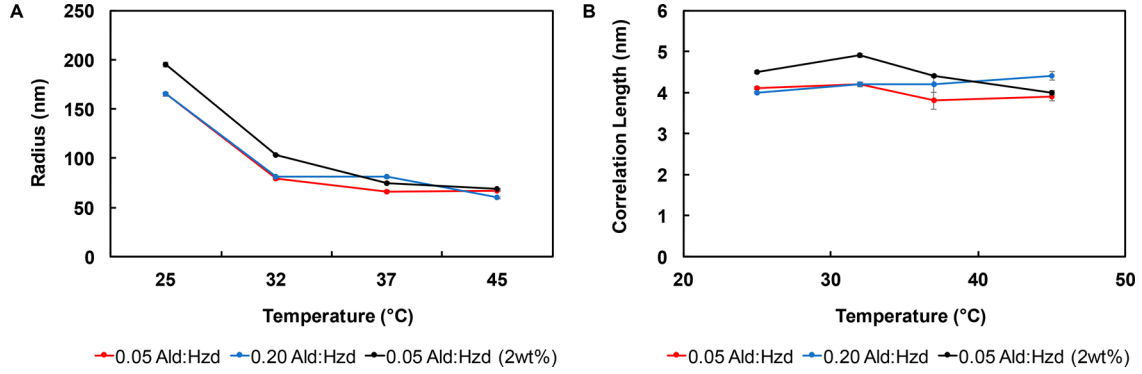

Figure 3. Key fitting parameters of the SANS analysis on bulk self-assembled PNIPAM microgels. (A) Microgel radius versus temperature; (B) correlation length versus temperature.

DOI: 10.1021/acs.langmuir.7b03664
Langmuir 2018, 34, 1601−1612

segregation is anticipated to be higher as the self-assembled microgels are heated compared to conventional microgels. As such, the correlation length may simultaneously track these different phenomena as the microgels are heated, making the trends less predictable. However, we also note that mesh size is difficult to measure accurately even with conventional PNIPAM microgels,[30] and the aggregation noted in the 0.20 Ald/Hzd microgel may also be skewing the results for that particular sample. Regardless, a homogeneous sphere model can give good fits to the SANS profiles of self-assembled microgels over the full transition range, suggesting that the internal morphology of these microgels is significantly more homogeneous than that of conventional microgels.

Contrast Matching Experiment. To independently track the distributions of PNIPAM-Ald and PNIPAM-Hzd within the microgel network, PNIPAM-Hzd was deuterium labeled by preparing the copolymer with d7-NIPAM as the monomer. Self-assembled microgels were then fabricated in appropriate index-matching solvents applicable to "hiding" each constituent component of the microgel network (63:37 D_2O/H_2O to hide PNIPAM-Hzd and 22:78 D_2O/H_2O to hide PNIPAM-Ald), allowing for unambiguous contrast matching of one component while preserving the scattering from the other component. USANS measurements were also performed on the same samples to allow for a further extension of the accessible q range and give additional confirmation of the quality of the model fits. Figure 4 shows the combined SANS and USANS curves, including the fits, for matched PNIPAM-Hzd and matched PNIPAM-Ald microgels as a function of temperature; the USANS data is highlighted with the dashed boxes to demonstrate the smooth transition at the low q region between the USANS and SANS ranges. Table 3 shows the key fitting parameters accessed from the resulting homogeneous sphere model fits. Refer to Supporting Information Table S5 for all fitting parameters used in IgorPro.

Aside from the higher background intensity of the PNIPAM-Ald index-matched profiles (a result of the higher amount of H_2O in the solvent mixture), the scattering profiles of both index matched polymers follow a remarkably similar shape (Figure 4). The homogeneous sphere model ($\sigma_{fuzzy} = 0$) again gave excellent fits to both index matched polymer distributions at all temperatures studied over the full accessible USANS/SANS q range. The best-fit radii of both index-matched polymer distributions decrease with temperature (as anticipated for PNIPAM-based materials, Table 3) and are quantitatively matched at each temperature regardless what polymer is index-matched, suggesting that both polymers are present throughout the whole mass of the microgel. In addition, although the absolute values of the

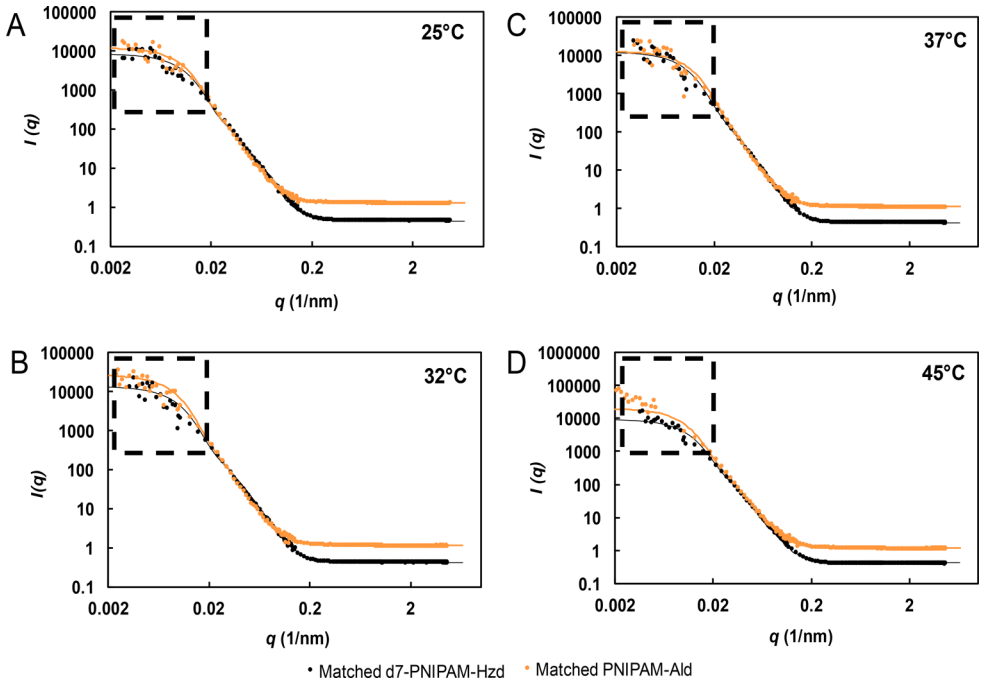

Figure 4. Combined SANS and USANS intensity versus q profiles (and fits) for index-matched d7-PNIPAM-Hzd (black curve) and index-matched PNIPAM-Ald (orange curve) in self-assembled microgels as a function of temperature (0.20 Ald/Hzd ratio, 1 wt % d7-PNIPAM-Hzd). USANS data are highlighted with a dotted black box. Note that while standard deviations of the fits are plotted as error bars, most error bars are too small to be visible on the graph.

Table 3. Best-Fit Parameters from Homogeneous Nekarnatwork Fits of the Combined USANS/SANS Data for Self-Assembled Microgels[a]

	25 °C		32 °C		37 °C		45 °C	
	(A)	(B)	(A)	(B)	(A)	(B)	(A)	(B)
radius (nm)	120	125	118	120	88	88	81	85
polydispersity	0.45	0.46	0.55	0.61	0.79	0.68	0.79	0.85
mesh size (nm)	30	34	30	34	30	34	30	32

[a]Fabricated with d7-PNIPAM-Hzd and PNIPAM-Ald examined using contrast matching experiments sequentially hiding (A) the d7-PNIPAM-Hzd polymer and (B) the PNIPAM-Ald polymer.

DOI: 10.1021/acs.langmuir.7b03664
Langmuir 2018, 34, 1601−1612

correlation lengths must be interpreted with extreme caution, as the inherent uncertainty in this value coupled with the fact that the contrast matching technique hides a significant fraction of the microgel mass in each experiment, the correlation lengths of the two contrast matched samples are very similar and again independent of temperature, suggesting that the feature sizes associated with both the d7-PNIPAM-Hzd and PNIPAM-Ald distributions are similar. All these observations are consistent with the oligomeric self-assembled microgels possessing a homogeneously cross-linked network structure.

It must be noted that the measured polydispersity values are significantly larger than those observed with the noncontrast matched experiment (Tables S3 and S4). While this result is likely in part simply a result of the contrast matching experiment itself, in which a large amount of the total mass of the microgel is "missing" in the scattering curve, the inherent differences in the LCST values between deuterated and protonated PNIPAM-Hzd may also promote larger polydispersities relative to those observed in the noncontrast matched samples. The LCST of the deuterated PNIPAM-Hzd in H_2O is ∼60 °C, compared to ∼56 °C for the protonated PNIPAM-Hzd; the addition of D_2O in the solvent (as required to index match the deuterated polymer) further increases the LCST values by 1−3 °C.[63] As such, given that the assembly temperature was identical for all assemblies (70 °C), the fabrication of d7-PNIPAM-Hzd-containing microgels occurred much closer to the LCST of the nanoaggregate seed polymer than assemblies using PNIPAM-Hzd. We have previously observed that assemblies performed close to the LCST of the seed polymer result in less defined nanoaggregates and thus more polydisperse microgels, as observed here.[2] However, because the mechanism of assembly remains the same, the results extracted here remain relevant to the all-protonated microgels. It should also be noted that the polydispersity values of the overall microgels are all reasonably low (PDI < 0.15) over the full size range tested for both 0.05 Ald/Hzd and 0.20 Ald/Hzd microgels in D_2O (Figure S4), making it more likely that this larger polydispersity is a fitting artifact rather than a real effect.

SANS of Self-Assembled Layered PNIPAM Microgels. To investigate how the addition of subsequent reactive polymers to a preassembled microgel (i.e., LbL modification) influences the internal morphology of the resulting microgels, SANS was used to probe the internal morphology of the resulting microgels. Table 4 shows the change in microgel radius as a function of adding sequential layers of PNIPAM-Hzd polymer or alternating layers of PNIPAM-Ald and PNIPAM-Hzd (see Supporting Information, Figure S5 for the raw SANS data and the best-fit curves). Full fitting parameters (including a summary) are provided in Supporting Information Table S6.

As with the self-assembled microgels themselves, no visual or quantitative (via χ^2 values, see Supporting Information Table S2) improvement in the quality of fit was achieved when using the fuzzy sphere model relative to a homogeneous sphere model, suggesting that the addition of the subsequent functional polymers does not substantially alter the homogeneity of the microgel network (i.e., a "shell" is not formed). However, consistent in terms of both trends as well as absolute radius values with the DLS results (Table 1), the best-fit radius slightly increased when an additional "layer" of PNIPAM-Hzd was added to a preassembled 0.05 Ald/Hzd (1 wt %) microgel. On the basis of these results, we hypothesize the observed size increase is a result not of the formation of a PNIPAM-Hzd-rich shell but rather a homogeneous increase in the hydrophilicity of the microgel network due to the introduction of an increasing number of unreacted polar hydrazide groups. Combined with the concurrent increase in total mass density within the microgel, the increased polarity increases the osmotic pressure inside the gel phase to drive swelling in the microgel, resulting in the larger measured size.

When a second polymer "layer" was added, the particle size did not significantly change regardless of whether the polymer was PNIPAM-Hzd or PNIPAM-Ald, although the reason behind each result is different. The original self-assembled microgels have a 20:1 excess of hydrazide versus aldehyde groups (0.05 Ald/Hzd); as such, the first PNIPAM-Hzd treatment can easily consume the available free (unreacted) aldehydes remaining from the assembly step, resulting in little if any of the additional PNIPAM-Hzd being cross-linked/immobilized into the microgel network. In contrast, the large excess hydrazide content means that the addition of further PNIPAM-Ald does result in the formation of more cross-links (less swelling) as well as the replacement of free hydrazide groups with either aldehydes or hydrazones, both of which are less polar. These dual deswelling responses are offset by the increase in net polymer concentration within the microgel phase (driving osmotic swelling) to result in no net change in microgel particle size upon the addition of the second layer. Regardless of the mechanisms involved, these results confirm that the homogeneous sphere model can accurately fit the internal structure of oligomeric self-assembled microgels regardless of how many subsequent additions of reactive prepolymer are performed. This result means that the prepolymers can freely diffuse into the preformed microgel instead of forming the dense core-diffuse shell structure that would have been anticipated in traditional layer-by-layer assembly.

Langmuir Trough. As a complementary method to probe the internal morphology of the microgels, surface pressure measurements of 0.05 Ald/Hzd (1 wt % PNIPAM-Hzd) and 0.20 Ald/Hzd (1 wt % PNIPAM-Hzd) self-assembled microgels assembled at the *n*-decane/water interface were performed using a Langmuir trough. Figure 5 shows the normalized compression isotherms (composed from different microgel concentrations) of these two self-assembled microgels in comparison to previously reported isotherms related to conventionally fabricated PNIPAM-*co*-methacrylic acid (PNIPAM-*co*-MAA) microgels that have previously been identified via SANS analysis to have a fuzzy sphere morphology.[38] Note that un-normalized compression

Table 4. Best-Fit Parameters from Homogeneous Network Fits of the SANS Data for Layer-by-Layer Self-Assembled Microgels[a]

microgel description	radius (nm)	polydispersity (%)	correlation length (nm)
0.05 Ald/Hzd (1 wt %)	165 ± 2	4	4.1
0.05 Ald/Hzd (1 wt %) + PNIPAM-Hzd	177 ± 1	8	4.5
0.05 Ald/Hzd (1 wt %) + PNIPAM-Hzd + PNIPAM-Hzd	178 ± 4	10	3.6
0.05 Ald/Hzd (1 wt %) + PNIPAM-Ald	167 ± 2	7	2.5
0.05 Ald/Hzd (1 wt %) + PNIPAM-Hzd + PNIPAM-Ald	176 ± 2	5	12.1

[a]Based on a 0.05 Ald/Hzd (1 wt % PNIPAM-Hzd) microgel core (solvent = D_2O), measured at 25°C.

DOI: 10.1021/acs.langmuir.7b03664
Langmuir 2018, 34, 1601−1612

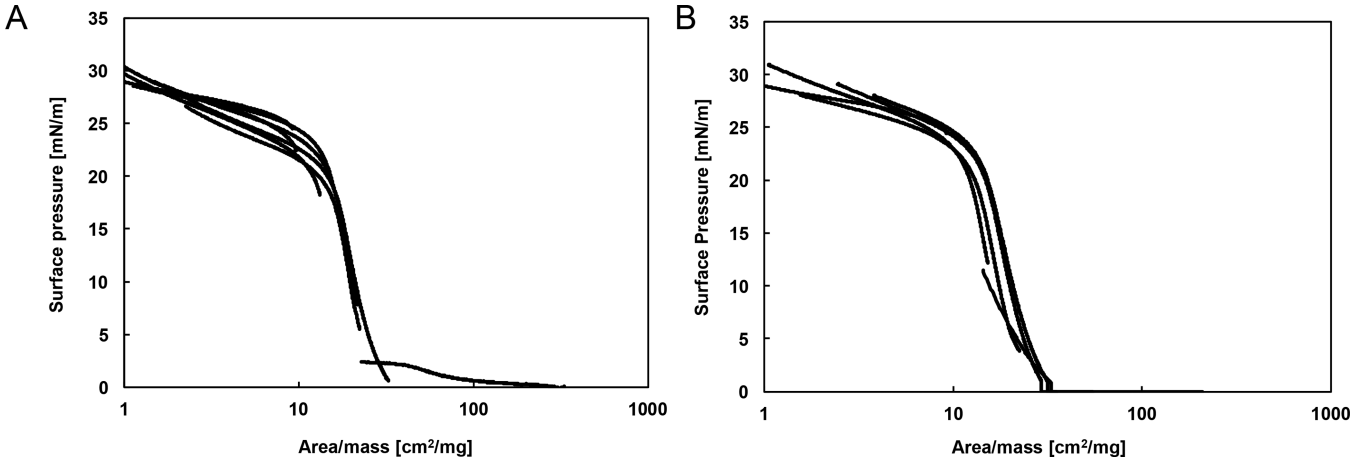

Figure 5. Normalized compression isotherms of self-assembled PNIPAM microgels (A) 0.05 Ald/Hzd (1 wt % PNIPAM-Hzd) and (B) 0.20 Ald/Hzd (1 wt % PNIPAM-Hzd) at the *n*-decane/water interface.

isotherms (with the corresponding amounts of 1 wt % microgel solution) are included as Supporting Information, Figure S6.

For the self-assembled microgels, the compression isotherms at different concentrations followed the same shape and reached a single plateau, independent of the cross-link ratio. We anticipate that the lack of difference between the 0.05 Ald/Hzd and 0.20 Ald/Hzd microgels is attributable to the reduction in the sensitivity of the Langmuir trough technique due to the moderate polydispersity of the self-assembled microgels, which cannot pack perfectly at the interface as do conventional microgels. In addition, both compression isotherms were sigmoidally shaped with only a single plateau observed upon compression. In contrast, conventionally fabricated PNIPAM microgels with a known dense core-disperse shell structure show a distinct second plateau at the higher range of surface pressures tested.[64,65] This type of iso-structural transition has been attributed to the differences in compression forces measured whether the microgels are in shell−shell contact (two more loosely cross-linked networks, compressible at lower forces) or core−core contact (two more tightly cross-linked networks, compressible only at higher forces).[65] The absence of this second plateau in self-assembled microgel data suggests that there is no such spatial difference in cross-linking density (i.e., no core−shell) in these microgels, again consistent with the successful SANS fits of these microgels as homogeneously cross-linked networks.

DISCUSSION

Controlling the internal morphology of microgels is essential to generating the swelling, diffusive, and interfacial properties required for specific applications. Herein, SANS (both with and without contrast matching of the constituent gel precursor polymers), USANS, and surface force measurements all suggest that our oligomeric self-assembled microgels have a homogeneously cross-linked structure, in contrast to PNIPAM microgels prepared using the conventional free radical precipitation polymerization technique. This result is somewhat unanticipated given the sequential addition synthetic procedure used to prepare the microgels starting from a preaggregated PNIPAM-Hzd seed above the phase transition temperature; the addition of a polymeric cross-linker to a collapsed nanoaggregate was expected to lead to the formation of a dense shell morphology based on the low anticipated diffusion of the PNIPAM-Ald cross-linker into the nanoaggregate. However, we believe the result presented is reasonable for two reasons. First, the self-assembly is conducted just above the lower critical solution temperature of what is a fairly polar starting material; ∼15 mol % of the monomeric units on PNIPAM-Hzd have a highly polar hydrazide group attached. As such, while it is clear from both DLS and the SANS measurements that nanoaggregation is occurring, the nanoaggregate is likely neither highly collapsed nor highly organized with the latter point supported by the substantial decrease in the polydispersity of the nanoaggregate upon cross-linking with PNIPAM-Ald (from ∼30% for the nanoaggregate to ∼10−20% for the bulk self-assembled PNIPAM microgels, Tables S3 and S4). As such, relative to unfunctionalized PNIPAM polymers that form highly condensed aggregates, the more polar PNIPAM-Hzd nanoaggregates can likely facilitate interdiffusion of the PNIPAM-Ald cross-linking polymer. Furthermore, since the assembly temperature is also higher than the LCST of the relatively small PNIPAM-Ald oligomer (M_n ∼ 15 kDa, LCST ∼ 42 °C), the diameter of collapsed PNIPAM-Ald chains would be small and the aldehyde cross-linking groups would be less sterically accessible under the self-assembly conditions, enabling improved penetration of the polymer into the PNIPAM-Hzd nanoaggregate. Second, unlike the permanent free radical cross-links formed using the conventional microgel fabrication technique, our use of reversible and dynamic hydrazone cross-linking chemistry enables dynamic changes in the cross-linking density over time until an equilibrium is reached. Note that the slightly acidic pH value of both the reaction mixture and obtained microgels (pH ∼ 5.5−6) is consistent with allowing such dynamic exchange on the observed time scale.[66] Consistent with prior observations on low molecular weight polyelectrolytes, diffusion of the PNIPAM-Ald cross-linker (or any of the LbL polymer treatments) into the microgel bulk is on this basis thermodynamically favorable, given that distributing the PNIPAM-Ald polymer throughout the microgel would sterically maximize the number of hydrazone cross-links that could be formed. Thus, the combination of these kinetic and thermodynamic contributions makes it reasonable to expect a relatively homogeneous cross-link distribution.

The homogeneous nature of these self-assembled microgels adds to the potential advantages of these microgels relative to conventional microgels in biomedical applications. In addition to the inherent degradability offered by the hydrazone cross-links, the uniform network structure should offer more predictable drug release rates, affinities to environmental analytes, or refractive properties for biosensor applications.

DOI: 10.1021/acs.langmuir.7b03664
Langmuir 2018, 34, 1601−1612

SUMMARY AND CONCLUSIONS

A combination of surface force measurements, SANS, and USANS was used to demonstrate that self-assembled microgels based on hydrazide and aldehyde-functionalized poly(*N*-isopropylacrylamide) oligomers have a homogeneously cross-linked internal structure. This structure is hypothesized to form as a result of the combination of the dynamic nature of the hydrazone cross-linking chemistry and the assembly conditions used that promote polymer interdiffusion. In contrast, conventional precipitation polymerization-derived PNIPAM microgels have a diffuse shell−dense core structure. As such, we anticipate that these well-defined degradable and homogeneous nanoscale gel networks offer opportunities for addressing challenges in drug delivery, biosensing, and optics by exploiting the predictable diffusive and refractive properties of the homogeneous microgel networks.

ASSOCIATED CONTENT

Supporting Information

The Supporting Information is available free of charge on the ACS Publications website at DOI: 10.1021/acs.langmuir.7b03664.

Raw and best-fit SANS profiles for all data presented, hydrodynamic diameter versus temperature profiles of the microgels collected in the SANS solvent(s), raw (unnormalized) Langmuir Trough compression data, and full tables summarizing the SANS best-fit parameters are provided (PDF)

AUTHOR INFORMATION

Corresponding Author

*E-mail: hoaretr@mcmaster.ca.

ORCID

Richard J. Alsop: 0000-0003-0563-0063

Walter Richtering: 0000-0003-4592-8171

Todd Hoare: 0000-0002-5698-8463

Notes

The authors declare no competing financial interest.

ACKNOWLEDGMENTS

Funding from the Natural Sciences and Engineering Research Council of Canada (NSERC, Discovery Grant Program RGPIN 356693) and the Ontario Early Researcher Awards (Ontario Ministry of Research and Innovation, ERA ER09-06-185) is gratefully acknowledged. Access to USANS BT5 and NGB30SANS was provided by the Center for High Resolution Neutron Scattering, a partnership between the National Institute of Standards and Technology and the National Science Foundation under Agreement No. DMR-1508249. E.M. acknowledges the receipt of the Ronald William Merkel Travel Scholarship and the Engineering Student Mobility Award from McMaster University to facilitate her travel to Germany as well as and Nadine Daleiden for help with the Langmuir trough experiments. A.S. acknowledges funding the Alexander von Humboldt Foundation. W.R. thanks the Deutsche Forschungsgemeinschaft for support within SFB 985 "Functional microgels and microgel systems". Certain commercial equipment, instruments, or materials are identified in this paper to foster understanding. Such identification does not imply recommendation or endorsement by the National Institute of Standards and Technology, nor does it imply that the materials or equipment identified are necessarily the best available for the purpose.

REFERENCES

(1) Wu, X.; Pelton, R. H.; Hamielec, A. E.; Woods, D. R.; McPhee, W. The kinetics of poly(N-isopropylacrylamide) microgel latex formation. *Colloid Polym. Sci.* **1994**, *272* (4), 467−477.

(2) Sivakumaran, D.; Mueller, E.; Hoare, T. Temperature-induced assembly of monodisperse, covalently cross-linked, and degradable poly (N-isopropylacrylamide) microgels based on oligomeric precursors. *Langmuir* **2015**, *31* (21), 5767−5778.

(3) Hoare, T.; Pelton, R. Highly pH and temperature responsive microgels functionalized with vinylacetic acid. *Macromolecules* **2004**, *37* (7), 2544−2550.

(4) Plamper, F. A.; Richtering, W. Functional Microgels and Microgel Systems. *Acc. Chem. Res.* **2017**, *50* (2), 131−140.

(5) Ngai, T.; Behrens, S. H.; Auweter, H. Novel emulsions stabilized by pH and temperature sensitive microgels. *Chem. Commun.* **2005**, *3*, 331−333.

(6) Hoare, T.; Pelton, R. Characterizing charge and crosslinker distributions in polyelectrolyte microgels. *Curr. Opin. Colloid Interface Sci.* **2008**, *13* (6), 413−428.

(7) Karg, M.; Pastoriza-Santos, I.; Rodriguez-Gonzalez, B.; von Klitzing, R.; Wellert, S.; Hellweg, T. Temperature, pH, and ionic strength induced changes of the swelling behavior of PNIPAM− poly (allylacetic acid) copolymer microgels. *Langmuir* **2008**, *24* (12), 6300−6306.

(8) Jones, C. D.; Lyon, L. A. Synthesis and characterization of multiresponsive core− shell microgels. *Macromolecules* **2000**, *33* (22), 8301−8306.

(9) Hoare, T. R.; Kohane, D. S. Hydrogels in drug delivery: progress and challenges. *Polymer* **2008**, *49* (8), 1993−2007.

(10) Zhang, Q.; Colazo, J.; Berg, D.; Mugo, S. M.; Serpe, M. J. Multiresponsive Nanogels for Targeted Anticancer Drug Delivery. *Mol. Pharmaceutics* **2017**, *14*, 2624.

(11) Yallapu, M. M.; Jaggi, M.; Chauhan, S. C. Design and engineering of nanogels for cancer treatment. *Drug Discovery Today* **2011**, *16* (9), 457−463.

(12) Sun, M.; Zhu, A.; Zhang, Q.; Ye, M.; Liu, Q. Smart shape-controlled synthesis of poly (N-isopropylacrylamide)/chitosan/Fe 3 O 4 microgels. *Eur. Polym. J.* **2015**, *66*, 569−576.

(13) Silva, C. S.; Baptista, R. P.; Santos, A. M.; Martinho, J. M.; Cabral, J. M.; Taipa, M. Â. Adsorption of human IgG on to poly (N-isopropylacrylamide)-based polymer particles. *Biotechnol. Lett.* **2006**, *28* (24), 2019−2025.

(14) Hoare, T.; Santamaria, J.; Goya, G. F.; Irusta, S.; Lin, D.; Lau, S.; Padera, R.; Langer, R.; Kohane, D. S. A magnetically triggered composite membrane for on-demand drug delivery. *Nano Lett.* **2009**, *9* (10), 3651−3657.

(15) Ogawa, K.; Wang, B.; Kokufuta, E. Enzyme-regulated microgel collapse for controlled membrane permeability. *Langmuir* **2001**, *17* (16), 4704−4707.

(16) Morones, J. R.; Frey, W. Room temperature synthesis of an optically and thermally responsive hybrid PNIPAM−gold nanoparticle. *J. Nanopart. Res.* **2010**, *12* (4), 1401−1414.

(17) Lu, Y.; Mei, Y.; Ballauff, M.; Drechsler, M. Thermosensitive core− shell particles as carrier systems for metallic nanoparticles. *J. Phys. Chem. B* **2006**, *110* (9), 3930−3937.

(18) Hoare, T.; Pelton, R. Impact of Microgel Morphology on Functionalized Microgel− Drug Interactions. *Langmuir* **2008**, *24* (3), 1005−1012.

(19) Guan, Y.; Zhang, Y. PNIPAM microgels for biomedical applications: from dispersed particles to 3D assemblies. *Soft Matter* **2011**, *7* (14), 6375−6384.

(20) Ungaro, F.; Giovino, C.; Catanzano, O.; Miro, A.; Mele, A.; Quaglia, F.; La Rotonda, M. I. Use of cyclodextrins as solubilizing agents for simvastatin: effect of hydroxypropyl-*β*-cyclodextrin on lactone/hydroxyacid aqueous equilibrium. *Int. J. Pharm.* **2011**, *404* (1), 49−56.

(21) Acciaro, R.; Gilányi, T.; Varga, I. Preparation of monodisperse poly (N-isopropylacrylamide) microgel particles with homogenous cross-link density distribution. *Langmuir* **2011**, *27* (12), 7917−7925.

(22) Tan, B. H.; Tam, K. C. Review on the dynamics and microstructure of pH-responsive nano-colloidal systems. *Adv. Colloid Interface Sci.* **2008**, *136* (1), 25−44.
(23) Jones, C. D.; Lyon, L. A. Shell-restricted swelling and core compression in poly (N-isopropylacrylamide) core− shell microgels. *Macromolecules* **2003**, *36* (6), 1988−1993.
(24) Dai, Z.; Ngai, T. Microgel particles: The structure-property relationships and their biomedical applications. *J. Polym. Sci., Part A: Polym. Chem.* **2013**, *51* (14), 2995−3003.
(25) Sanson, N.; Rieger, J. Synthesis of nanogels/microgels by conventional and controlled radical crosslinking copolymerization. *Polym. Chem.* **2010**, *1* (7), 965−977.
(26) Sivakumaran, D.; Maitland, D.; Hoare, T. Injectable microgel-hydrogel composites for prolonged small-molecule drug delivery. *Biomacromolecules* **2011**, *12* (11), 4112−4120.
(27) Pich, A.; Richtering, W. Microgels by Precipitation Polymerization: Synthesis, Characterization, and Functionalization. In *Chemical Design of Responsive Microgels*; Pich, A., Richtering, W., Eds.; Springer Berlin Heidelberg: Berlin, Heidelberg, 2011; pp 1−37.
(28) Kureha, T.; Sato, T.; Suzuki, D. Relationship between Temperature-Induced Changes in Internal Microscopic Structures of Poly (N-isopropylacrylamide) Microgels and Organic Dye Uptake Behavior. *Langmuir* **2014**, *30* (29), 8717−8725.
(29) Richtering, W.; Berndt, I.; Pedersen, J. S. Determination of Microgel Structure by Small-Angle Neutron Scattering. *Microgel Suspensions: Fundamentals and Applications* **2011**, 117−132.
(30) Stieger, M.; Pedersen, J. S.; Lindner, P.; Richtering, W. Are thermoresponsive microgels model systems for concentrated colloidal suspensions? A rheology and small-angle neutron scattering study. *Langmuir* **2004**, *20* (17), 7283−7292.
(31) Berndt, I.; Pedersen, J. S.; Richtering, W. Temperature-Sensitive Core−Shell Microgel Particles with Dense Shell. *Angew. Chem.* **2006**, *118* (11), 1769−1773.
(32) Saunders, B. R. On the structure of poly (N-isopropylacrylamide) microgel particles. *Langmuir* **2004**, *20* (10), 3925−3932.
(33) Kratz, K.; Hellweg, T.; Eimer, W. Structural changes in PNIPAM microgel particles as seen by SANS, DLS, and EM techniques. *Polymer* **2001**, *42* (15), 6631−6639.
(34) Meyer, S.; Richtering, W. Influence of polymerization conditions on the structure of temperature-sensitive poly (N-isopropylacrylamide) microgels. *Macromolecules* **2005**, *38* (4), 1517−1519.
(35) Pelton, R.; Chibante, P. Preparation of aqueous latices with N-isopropylacrylamide. *Colloids Surf.* **1986**, *20* (3), 247−256.
(36) Virtanen, O.; Brugnoni, M.; Kather, M.; Pich, A.; Richtering, W. The next step in precipitation polymerization of N-isopropylacrylamide: particle number density control by monochain globule surface charge modulation. *Polym. Chem.* **2016**, *7* (32), 5123−5131.
(37) Hoare, T.; McLean, D. Kinetic prediction of functional group distributions in thermosensitive microgels. *J. Phys. Chem. B* **2006**, *110* (41), 20327−20336.
(38) Geisel, K.; Isa, L.; Richtering, W. The Compressibility of pH-Sensitive Microgels at the Oil−Water Interface: Higher Charge Leads to Less Repulsion. *Angew. Chem., Int. Ed.* **2014**, *53* (19), 4905−4909.
(39) Hoare, T.; Pelton, R. Functionalized microgel swelling: comparing theory and experiment. *J. Phys. Chem. B* **2007**, *111* (41), 11895−11906.
(40) Xue, J.; Zhang, Z.; Nie, J.; Du, B. Formation of Microgels by Utilizing the Reactivity of Catechols with Radicals. *Macromolecules* **2017**, *50* (14), 5285−5292.
(41) Sheikholeslami, P.; Ewaschuk, C. M.; Ahmed, S. U.; Greenlay, B. A.; Hoare, T. Semi-batch control over functional group distributions in thermoresponsive microgels. *Colloid Polym. Sci.* **2012**, *290* (12), 1181−1192.
(42) Vo, C. D.; Kuckling, D.; Adler, H.-J.; Schönhoff, M. Preparation of thermosensitive nanogels by photo-cross-linking. *Colloid Polym. Sci.* **2002**, *280* (5), 400−409.
(43) Kuckling, D.; Vo, C. D.; Wohlrab, S. E. Preparation of nanogels with temperature-responsive core and pH-responsive arms by photo-cross-linking. *Langmuir* **2002**, *18* (11), 4263−4269.
(44) Cao, Z.; Du, B.; Chen, T.; Nie, J.; Xu, J.; Fan, Z. Preparation and properties of thermo-sensitive organic/inorganic hybrid microgels. *Langmuir* **2008**, *24* (22), 12771−12778.
(45) Oh, J. K.; Tang, C.; Gao, H.; Tsarevsky, N. V.; Matyjaszewski, K. Inverse miniemulsion ATRP: a new method for synthesis and functionalization of well-defined water-soluble/cross-linked polymeric particles. *J. Am. Chem. Soc.* **2006**, *128* (16), 5578−5584.
(46) Oh, J. K.; Bencherif, S. A.; Matyjaszewski, K. Atom transfer radical polymerization in inverse miniemulsion: a versatile route toward preparation and functionalization of microgels/nanogels for targeted drug delivery applications. *Polymer* **2009**, *50* (19), 4407−4423.
(47) Duncanson, W. J.; Lin, T.; Abate, A. R.; Seiffert, S.; Shah, R. K.; Weitz, D. A. Microfluidic synthesis of advanced microparticles for encapsulation and controlled release. *Lab Chip* **2012**, *12* (12), 2135−2145.
(48) Wong, J. E.; Richtering, W. Layer-by-layer assembly on stimuli-responsive microgels. *Curr. Opin. Colloid Interface Sci.* **2008**, *13* (6), 403−412.
(49) Kleinen, J.; Klee, A.; Richtering, W. Influence of architecture on the interaction of negatively charged multisensitive poly (N-isopropylacrylamide)-co-methacrylic acid microgels with oppositely charged polyelectrolyte: absorption vs adsorption. *Langmuir* **2010**, *26* (13), 11258−11265.
(50) Kleinen, J.; Richtering, W. Rearrangements in and release from responsive microgel− polyelectrolyte complexes induced by temperature and time. *J. Phys. Chem. B* **2011**, *115* (14), 3804−3810.
(51) Deng, X.; Smeets, N. M.; Sicard, C. m.; Wang, J.; Brennan, J. D.; Filipe, C. D.; Hoare, T. Poly (oligoethylene glycol methacrylate) Dip-Coating: Turning Cellulose Paper into a Protein-Repellent Platform for Biosensors. *J. Am. Chem. Soc.* **2014**, *136* (37), 12852−12855.
(52) Smeets, N. M.; Bakaic, E.; Patenaude, M.; Hoare, T. Injectable and tunable poly (ethylene glycol) analogue hydrogels based on poly (oligoethylene glycol methacrylate). *Chem. Commun.* **2014**, *50* (25), 3306−3309.
(53) Patenaude, M.; Campbell, S.; Kinio, D.; Hoare, T. Tuning Gelation Time and Morphology of Injectable Hydrogels Using Ketone−Hydrazide Cross-Linking. *Biomacromolecules* **2014**, *15* (3), 781−790.
(54) Azuah, R. T.; Kneller, L. R.; Qiu, Y.; Tregenna-Piggott, P. L.; Brown, C. M.; Copley, J. R.; Dimeo, R. M. DAVE: a comprehensive software suite for the reduction, visualization, and analysis of low energy neutron spectroscopic data. *J. Res. Natl. Inst. Stand. Technol.* **2009**, *114* (6), 341.
(55) Kline, S. R. Reduction and analysis of SANS and USANS data using IGOR Pro. *J. Appl. Crystallogr.* **2006**, *39* (6), 895−900.
(56) Yuan, G.; Luo, J.; Han, C. C.; Liu, Y. Gelation transitions of colloidal systems with bridging attractions. *Phys. Rev. E* **2016**, *94* (4), 040601.
(57) Pedersen, J. S.; Posselt, D.; Mortensen, K. Analytical treatment of the resolution function for small-angle scattering. *J. Appl. Crystallogr.* **1990**, *23* (4), 321−333.
(58) Horkay, F.; Hammouda, B. Small-angle neutron scattering from typical synthetic and biopolymer solutions. *Colloid Polym. Sci.* **2008**, *286* (6−7), 611−620.
(59) Grobelny, S.; Hofmann, C. H.; Erlkamp, M.; Plamper, F. A.; Richtering, W.; Winter, R. Conformational changes upon high pressure induced hydration of poly (N-isopropylacrylamide) microgels. *Soft Matter* **2013**, *9* (25), 5862−5866.
(60) Smeets, N. M.; Bakaic, E.; Yavitt, F. M.; Yang, F.-C.; Rheinstädter, M. C.; Hoare, T. Probing the Internal Morphology of Injectable Poly (oligoethylene Glycol Methacrylate) Hydrogels by Light and Small-Angle Neutron Scattering. *Macromolecules* **2014**, *47* (17), 6017−6027.
(61) Höfl, S.; Zitzler, L.; Hellweg, T.; Herminghaus, S.; Mugele, F. Volume phase transition of "smart" microgels in bulk solution and adsorbed at an interface: a combined AFM, dynamic light, and small angle neutron scattering study. *Polymer* **2007**, *48* (1), 245−254.

DOI: 10.1021/acs.langmuir.7b03664
Langmuir 2018, 34, 1601−1612

(62) Varga, I.; Gilányi, T.; Meszaros, R.; Filipcsei, G.; Zrínyi, M. Effect of cross-link density on the internal structure of poly (N-isopropylacrylamide) microgels. *J. Phys. Chem. B* **2001**, *105* (38), 9071−9076.
(63) Crowther, H. M.; Saunders, B. R.; Mears, S. J.; Cosgrove, T.; Vincent, B.; King, S. M.; Yu, G.-E. Poly (NIPAM) microgel particle de-swelling: a light scattering and small-angle neutron scattering study. *Colloids Surf., A* **1999**, *152* (3), 327−333.
(64) Pinaud, F.; Geisel, K.; Massé, P.; Catargi, B.; Isa, L.; Richtering, W.; Ravaine, V.; Schmitt, V. Adsorption of microgels at an oil−water interface: correlation between packing and 2D elasticity. *Soft Matter* **2014**, *10* (36), 6963−6974.
(65) Rey, M.; Fernández-Rodríguez, M. Á.; Steinacher, M.; Scheidegger, L.; Geisel, K.; Richtering, W.; Squires, T. M.; Isa, L. Isostructural solid−solid phase transition in monolayers of soft core−shell particles at fluid interfaces: structure and mechanics. *Soft Matter* **2016**, *12* (15), 3545−3557.
(66) Rodriguez-Docampo, Z.; Otto, S. Orthogonal or simultaneous use of disulfide and hydrazone exchange in dynamic covalent chemistry in aqueous solution. *Chem. Commun.* **2008**, No. 42, 5301−5303.

DOI: 10.1021/acs.langmuir.7b03664
Langmuir 2018, 34, 1601−1612